Biosignatures as revealed by spectropolarimetry of Earthshine

Michael F. Sterzik[1], Stefano Bagnulo[2] & Enric Palle[3]

Low-resolution intensity spectra of Earth's atmosphere obtained from space reveal strong signatures of life ('biosignatures'), such as molecular oxygen and methane with abundances far from chemical equilibrium, as well as the presence of a 'red edge' (a sharp increase of albedo for wavelengths longer than 700 nm) caused by surface vegetation[1]. Light passing through the atmosphere is strongly linearly polarized by scattering (from air molecules, aerosols and cloud particles) and by reflection (from oceans and land[2]). Spectropolarimetric observations of local patches of Earth's sky light from the ground contain signatures of oxygen, ozone and water, and are used to characterize the properties of clouds and aerosols[3,4]. When applied to exoplanets, ground-based spectropolarimetry can better constrain properties of atmospheres and surfaces than can standard intensity spectroscopy[5-9]. Here we report disk-integrated linear polarization spectra of Earthshine, which is sunlight that has been first reflected by Earth and then reflected back to Earth by the Moon[10-13]. The observations allow us to determine the fractional contribution of clouds and ocean surface, and are sensitive to visible areas of vegetation as small as 10 per cent. They represent a benchmark for the diagnostics of the atmospheric composition, mean cloud height and surfaces of exoplanets.

Broadband polarimetric measurements of the disk-integrated Earth have been obtained previously[14]. Observations of Earthshine at a wavelength of 550 nm reported a fraction of linear polarization of about 10% for a Sun–Earth–Moon phase angle near to $90°$ (quadrature). As the lunar surface is responsible for a depolarization of the incident light by a factor of ~3.3, the true linear polarization of the disk-integrated light of Earth was estimated to be around 30–35% (ref. 14). Modern estimates of the Earth's linear polarization are based on measurements by the satellite-borne instrument POLDER in three bands (443 nm, 670 nm and 865 nm), and demonstrate strong dependence on cloud cover and on wavelength[15]. These measurements, however, do not allow a spectral analysis, and therefore cannot be used to infer biosignatures.

Using the Focal Reducer/Low-dispersion Spectrograph (FORS)[16] mounted at the Very Large Telescope in Chile, we measured the linear polarization spectra of Earthshine. Our data were collected during two observing epochs with distinct viewing geometries of Earth (observing techniques and data reduction details are given in Supplementary Information). A detailed breakdown of the surfaces visible in our Earthshine observations, derived from MODIS satellite observations[17], is given in Table 1.

The red curves in Figs 1 and 2 display the wavelength (λ) dependence of the fraction of linear polarization, $P_Q(\lambda)$ ($=Q/I$, the polarized flux Q over the total flux I, see the definition of the Stokes parameters in Supplementary Information), measured in April (Fig. 1) and in June (Fig. 2). The shape of the $P_Q(\lambda)$ profile depends mainly on Earth's surface albedo at the time of observations. On 25 April 2011, the continuum polarization reaches about 9% at 500 nm, and decreases smoothly to 4% at 900 nm. The polarization observed on 10 June 2011 is 3% higher than observed in April. A change of the continuum slope occurs visibly in the June spectrum at a wavelength of around 520 nm.

In particular, the June spectrum matches the observation by Dollfus[14] of 10% Earthshine polarization at his observing wavelength of 550 nm, whereas our April value is smaller. In order to display the detailed structure on top of the smooth continuum, we have fitted and subtracted from the observed $P_Q(\lambda)$ profile a fourth-order polynomial (between 530 and 910 nm). The residual signal $\delta P(\lambda)$ shows a rich structure at the 0.1% level. A narrow O_2 A-band (760 nm) is prominent in both spectra at a level of almost 1% above the continuum. O_2 B (690 nm) and H_2O (720 and 820 nm) bands are broader and with lower amplitude. An additional (strong) polarization feature is present in the June spectrum close to 850 nm, and a (weak) feature at 854 nm. We tentatively attribute them to the presence of a variable, thin Ca II layer in Earth's ionosphere, recently discovered through observations of the transmitted spectrum of the Earth[18]. Remarkably, the overall shape of the residuals between 550 and 750 nm differs between the two epochs: whereas the April spectrum exhibits a broad, shallow peak around 700 nm, the June spectrum appears rather flat.

We compared our measurements with the polarization estimated from POLDER data[15], and with published tables of radiative transfer models of Earth-like extrasolar planets[5]. For comparison purposes, both POLDER data and model predictions have to be scaled to account for the depolarization of the Earthshine caused by reflection from the

Table 1 | Earth observations

Observations	Observing date	
	25 April 2011, 09:00 UT	10 June 2011, 01:00 UT
View of Earth as seen from the Moon		
Sun–Earth–Moon phase (degrees)	87	102
Ocean fraction in Earthshine (%)	18	46
Vegetation fraction in Earthshine (%)	7	3
Tundra, shrub, ice and desert fraction in Earthshine (%)	3	1
Total cloud fraction in Earthshine (%)	72	50
Cloud fraction $\tau > 6$ (%)	42	27

This Table gives the contribution of different types of surface to the Earthshine, determined by mapping satellite cloud retrievals from MODIS on the parts of the Earth's surface that are visible from the Moon at the given observing epoch[17]. The first observing epoch was before dawn on 25 April 2011, and the Earthshine contains contributions from the Atlantic Ocean, the Amazonas region, and parts of Europe and Africa. The second observing epoch was after dusk on 10 June 2011, and probes the Pacific side of the Earth, with almost no visible land surfaces. The contribution to the Earthshine signal of a given Earth region will depend on the solar and lunar zenith angles (the reflectance is a bi-directional property), thus the percentage scene types and cloud cover fractions in the Table have been averaged over the whole Earthshine-contributing area using these weights[13]. The contributions of clear tundra, shrub, desert or ice scenes were negligible.

[1]European Southern Observatory, Alonso de Cordova 3107, Vitacura, Santiago, Chile. [2]Armagh Observatory, College Hill, Armagh BT61 9DG, UK. [3]Instituto de Astrofisica de Canarias, Via Lactea s/n, E38205 La Laguna, Tenerife, Spain.
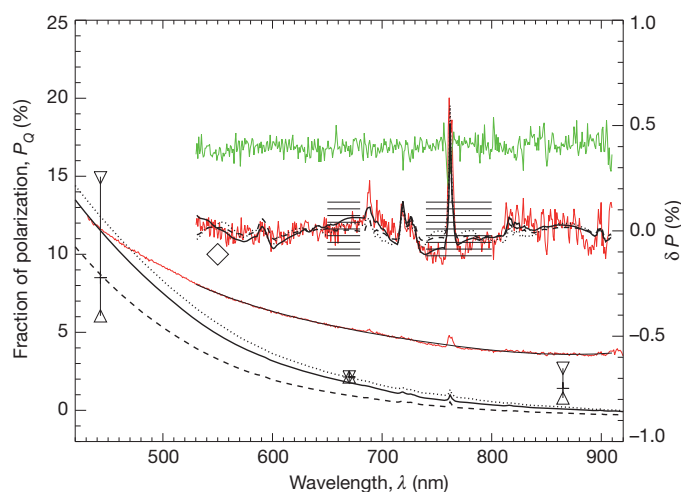
Figure 1 | Polarization spectra observed on 25 April 2011. Red lines show observed fractional polarization P_Q, black lines show model spectra for comparison. Both continuum polarization and residual polarization (derived from the continuum by subtracting a polynomial fitted in the wavelength region between 530 and 910 nm) are plotted with different scale units on the left and right axis to zoom in on the spectral fine-structure. For direct comparison with the Earthshine, the model spectra have been reduced in amplitude to account for the depolarization caused by the lunar surface[19,20]; the different linestyles refer to different choices of the model parameters (Table 2). The green line refers to the measured Stokes P_U as explained in the Supplementary Information (same scale as the residuals on the right axis), and is representative for the noise level in the spectra. Horizontal hatching between 650–680 nm and 740–800 nm denotes the NDVI bandpass regions and refers to the corresponding residual polarizations. Open triangles, POLDER-based whole-Earth polarization estimates at 443 nm, 670 nm and 865 nm with a mean cloud coverage of 55%; upper and lower triangles bracket low (10%) or high (90%) cloud coverage levels. Open diamond, Dollfus's estimate of an Earthshine polarization of 10% at a phase angle of 80° at 550 nm. An NDVI contrast is visible in the data and for model 'a', which is consistent with a 10–15% visible vegetation content in the Earthshine.

lunar surface. The lunar depolarization factor is not well determined, but roughly correlates with the albedo of the reflecting surfaces[19,20]. Following a classic study[14], we assume a linear increase of depolarization (depol) with wavelength, normalized to 3.3 at a wavelength at 550 nm (depol = $3.3\lambda/550$, where λ is in units of nm).

The interpretation of the POLDER data depends on the cloud coverage at the time of observation and is roughly consistent with our continuum values in April, but too low in June. The higher
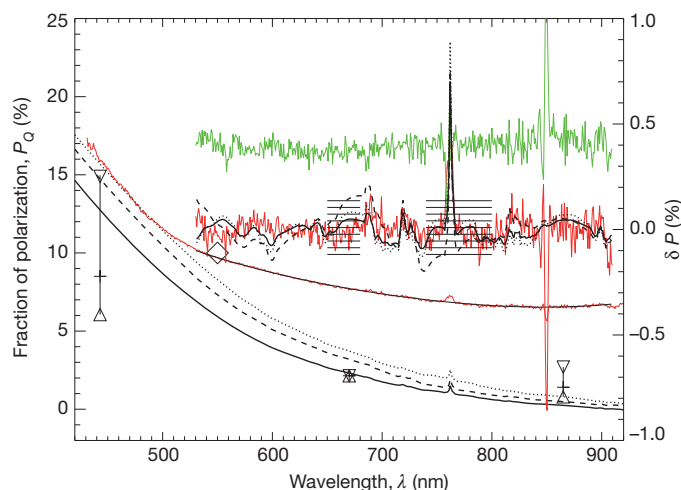
Figure 2 | Polarization spectra observed on 10 June 2011. Lines and symbols as for Fig. 1. An NDVI contrast is not evident in the data, and models 'a' and 'c' are consistent with no visible vegetation content in the Earthshine.

polarization we observed in June can be qualitatively explained by an approximately 20% lower cloud coverage during our Earthshine measurements than assumed for the disk-integration of the POLDER data[15].

For the comparisons with theoretical predictions, we constructed a fine grid of possible Earth spectra from published tables by varying the parameters in steps of 1% for the different scene types[5] (ocean clouded or clear, and vegetation clouded or clear). Then we compared these models with our observations in the wavelength region between 420 nm and 530 nm. In the blue spectral range, the effect of cloud properties on polarization is minor[21], and synthetic Earth model polarized spectra agree quantitatively with our observations. The parameters of the best fitting models are listed in Table 2 (April c and June c). For both observing epochs, the modelling results match MODIS-derived cloud coverage fractions calculated for clouds having optical depth $\tau > 6$. The June model—less affected by clouds—approximates the continuum well. However, the models[5] systematically predict polarizations in the red part of the continuum that are too low, primarily because of the approximations used in the models for the cloud microphysics[22]. Real clouds are patchy and, in particular over the ocean, exhibit much larger mean effective radii (droplet sizes 12–15 μm) and a high variation in their optical depth distribution[23]. Depending on the underlying surface types, higher polarization fractions are thus expected.

Guided by the actual observed surface scene fractions (Table 1), we have calculated more polarization spectra from tabulated model spectra[5] with parameters that are other plausible approximations to the real surface fractions responsible for the Earthshine spectrum at the epoch of the observations (model class parameters 'a' and 'b'). Although these models fail to explain the continuum, their residual profiles (generated with the same fourth-order polynomial fit and subtraction from the continuum as adopted as for the observed spectra) are consistent with our observations.

In Figs 1 and 2, we have hatched (horizontal lines) two bandpass regions at 650–680 nm and 740–800 nm and calculated the normalized difference vegetation index (NDVI)[24]. A larger contrast in the continuum averages in April than in June is interpreted by the presence of a strong vegetation 'red edge' signal in April, which is practically undetected in June. This feature in the April spectra can be reproduced by assuming about 10–15% cloud-free land vegetation (model April a of Table 2). A smaller fraction (models April b and c) reduces the NDVI contrast too much, while too large a fraction would over-estimate the observed feature. Similarly, the June data can best be described through little or absent cloud-free vegetation surfaces (models June a and c), while a 10% cloud-free vegetation fraction produces a NDVI that is too pronounced to be compatible with the data (model June b). We estimate that our data are sensitive to variations of 5% in the NDVI. Also, the observed polarization peak of the O_2 A feature (and to a lesser extent, O_2 B) is fully compatible with the models. The amplitude of these features are sensitive to the top of the cloud layer, and to the O_2 mixing ratio. Our Earthshine observations suggest a low top-layer (around 800 hPa), assuming the mixing ratio on Earth to be fixed[5]. The H_2O and O_3 (580 nm) band strengths also appear fully consistent with the model.

Table 2 | Model parameters

Model	Ocean clouded (%)	Ocean clear (%)	Vegetation clouded (%)	Vegetation clear (%)	Line in Fig. 2
April a	48	40	0	12	Solid
April b	60	30	10	0	Dashed
April c	44	56	0	0	Dotted
June a	40	60	0	0	Solid
June b	30	60	0	10	Dashed
June c	27	73	0	0	Dotted

This Table gives fractions of different types of surfaces used to model polarization spectra published in tables in ref. 5. Parameters for 'a' and 'b' models (leftmost column) are guided by observed scene type fractions in Table 1. The 'c' models are generated through a grid of synthetic spectra and fit the observations best within 420 and 530 nm. Note that the ocean clouded fractions agree well with the observed cloud fractions for optical depths $\tau > 6$ in Table 1.

Our spectropolarimetric measurements of the Earthshine constrain the Earth's surface and atmospheric composition and biosignatures. Improved vector radiative transfer models with more realistic cloud and surface treatment are necessary to fully account for the observed spectra. Validation of these models is necessary to interpret Earth-like exoplanet polarization spectra.

1. Sagan, C., Thompson, W. R., Carlson, R., Gurnett, D., &. Hord, C. A search for life on Earth from the Galileo spacecraft. *Nature* **365,** 715–721 (1993).
2. Coffeen, D. L. Polarization and scattering characteristics in the atmospheres of Earth, Venus, and Jupiter. *J. Opt. Soc. Am.* **69,** 1051–1064 (1979).
3. Aben, I., Helderman, F., Stam, D. M. & Stammes, P. Spectral fine-structure in the polarization of skylight. *Geophys. Res. Lett.* **26,** 591–594 (1999).
4. Boesche, E. *et al.* Polarization of skylight in the O_2A band: effects of aerosol properties. *Appl. Opt.* **47,** 3467–3480 (2008).
5. Stam, D. M. Spectropolarimetric signatures of Earth-like extrasolar planets. *Astron. Astrophys.* **482,** 989–1007 (2008).
6. Buenzli, E. & Schmid, H. M. A grid of polarization models for Rayleigh scattering planetary atmospheres. *Astron. Astrophys.* **504,** 259–276 (2009).
7. Keller, C. U. *et al.* EPOL: the exoplanet polarimeter for EPICS at the E-ELT. *Proc. SPIE* **7735,** 77356G (2010).
8. Bailey, J. Rainbows, polarization, and the search for habitable planets. *Astrobiology* **7,** 320–332 (2007).
9. Williams, D. M. & Gaidos, E. Detecting the glint of starlight on the oceans of distant planets. *Icarus* **195,** 927–937 (2008).
10. Arnold, L., Gillet, S., Lardiere, O., Riaud, P. & Schneider, J. A test for the search for life on extrasolar planets. Looking for the terrestrial vegetation signature in the Earthshine spectrum. *Astron. Astrophys.* **392,** 231–237 (2002).
11. Woolf, N. J., Smith, P. S., Traub, W. A. & Jucks, K. W. The spectrum of Earthshine: a pale blue dot observed from the ground. *Astrophys. J.* **574,** 430–433 (2002).
12. Seager, S., Turner, E. L., Schafer, J. & Ford, E. B. Vegetation's red edge: a possible spectroscopic biosignature of extraterrestrial plants. *Astrobiology* **5,** 372–390 (2005).
13. Montanes-Rodriguez, P., Palle, E., Goode, P. R. & Martin-Torres, F. J. Vegetation signature in the observed globally integrated spectrum of Earth considering simultaneous cloud data: applications for extrasolar planets. *Astrophys. J.* **651,** 544–552 (2006).
14. Dollfus, A. Études des planètes par la polarisation de leur lumière. *Suppléments aux Annales d'Astrophysique* **4,** 3–114 (1957).
15. Wolstencroft, R. D. & Breon, F.-M. in *Astronomical Polarimetry: Current Status and Future Directions* (eds Adamson, A., Aspin, C., Davis, C. J. & Fujiyoshi, T.) 211–212 (ASP Conf. Ser. Vol. 343, Astronomical Society of the Pacific, 2005).
16. Appenzeller, I. *et al.* Successful commissioning of FORS1 — the first optical instrument on the VLT. *ESO Messenger* **94,** 1–6 (1998).
17. Giovanni portal. http://disc.sci.gsfc.nasa.gov/giovanni/overview/index.html.
18. Pallé, E., Zapatero Osorio, M. R., Barrena, R., Montanes-Rodriguez, P. & Martin, E. L. Earth's transmission spectrum from lunar eclipse observations. *Nature* **459,** 814–816 (2009).
19. Fox, G. K. *et al.* Solar system observations by the Wisconsin Ultraviolet Photopolarimeter Experiment — III. The first ultraviolet linear spectropolarimetry of the Moon. *Mon. Not. R. Astron. Soc.* **298,** 303–309 (1998).
20. Shkuratov, Y. *et al.* Optical measurements of the Moon as a tool to study its surface. *Planet. Space Sci.* **59,** 1326–1371 (2011).
21. Goloub, P., Deuze, J. L., Herman, M. & Fouquart, Y. Analysis of the POLDER polarization measurements performed over cloud covers. *IEEE Trans. Geosci. Rem. Sens.* **32,** 78–88 (1994).
22. Karalidi, T., Stam, D. M. & Hovenier, J. W. Flux and polarisation spectra of water clouds on exoplanets. *Astron. Astrophys.* **530,** A69 (2011).
23. Kokhanovsky, A., Platnick, S. & King, M. D. in *The Remote Sensing of Tropospheric Composition from Space* (eds Burrows, J. P. *et al.*) 231–257 (Springer, 2011).
24. Tinetti, G. *et al.* Detectability of planetary characteristics in disk-averaged spectra II: synthetic spectra and light-curves of Earth. *Astrobiology* **6,** 881–900 (2006).

Supplementary Information is linked to the online version of the paper at www.nature.com/nature.

Author Contributions M.F.S. was the principal investigator of the programme, contributing to observation preparation and execution, data analysis and interpretation, comparison with models, and writing of the manuscript. S.B. was a co-investigator, contributing to observation preparation and execution, data reduction and interpretation, error analysis, comparison with models, and also contributing to the manuscript. E.P. was a co-investigator, contributing to observation preparation, data interpretation, and derivations of actual Earth surface fractions during the observations.

Author Information Reprints and permissions information is available at www.nature.com/reprints. The authors declare no competing financial interests. Readers are welcome to comment on the online version of this article at www.nature.com/nature. Correspondence and requests for materials should be addressed to M.F.S. (msterzik@eso.org).